Letter | Editors' Suggestion

Dimer problem on a spherical surface

A. Tononi [1], D. S. Petrov [2], and M. Lewenstein [1,3]

[1] *ICFO-Institut de Ciencies Fotoniques, The Barcelona Institute of Science and Technology, 08860 Castelldefels (Barcelona), Spain*

[2] *Université Paris-Saclay, CNRS, LPTMS, 91405 Orsay, France*

[3] *ICREA, Pg. Lluís Companys 23, 08010 Barcelona, Spain*

(Received 10 February 2025; accepted 28 April 2025; published 19 May 2025)

We solve the problem of a dimer moving on a spherical surface and find that its binding energy and wave function are sensitive to the total angular momentum. The dimer gets squeezed in the direction orthogonal to the center-of-mass motion and can qualitatively change its geometry from two dimensional to one dimensional. These results suggest that combining the curved geometry with finite angular momentum may give rise to qualitatively new many-body phenomena in ultracold shell-shaped gases.

DOI: 10.1103/PhysRevA.111.L051304

The problem of two interacting bodies has a central importance in diverse areas of physics ranging from celestial mechanics and general relativity [1–3] to classical electrodynamics [4]. In quantum mechanics, it underlies the solution of the hydrogen atom and the theory of scattering [5]. Two-body physics also rules the thermodynamic description of ultracold atomic gases [6,7] since their interaction range is much smaller than their de Broglie wavelengths and average interparticle distances. In particular, the zero-range scattering problem has been solved in three-dimensional free space [5], in quasi-one-dimensional [8] and in quasi-two-dimensional [9] geometries, and the spectrum of a harmonically confined pair of atoms was obtained in any spatial dimension [10]. These solutions are crucial for understanding Feshbach resonances in trapped gases [11,12], the crossover from the Bardeen-Cooper-Schrieffer state to the Bose-Einstein condensate of molecules (BCS-BEC crossover) in fermionic mixtures [13], two-dimensional universal thermodynamics [14,15], solitons and nonlinear states [16,17], and many other phenomena in ultracold gases.

In the above cases, the solution of the two-body problem is simplified by its *separability* into two independent single-particle problems: one for the center-of-mass free dynamics, another for the relative motion of the particles. The separability is however not assured if the particles are constrained to move in optical lattices [18,19], in mixed-dimensional setups [20–23], in anharmonic [24,25] or species-dependent harmonic [26,27] potentials, or in spatial domains which are compact or curved. In particular, solving the two-body problem in curved setups is more difficult than in flat counterparts, but fundamentally valuable for discovering new quantum-mechanical behaviors induced by the curved geometry [28]. Indeed, the solution of one- and two-body problems on a spherical surface evinced interesting consequences associated with curvature and to nonseparability. For instance, there were studies of p-wave dimers moving under a geometrically induced gauge field [29], of s-wave scattering of one body [30] and of two bodies on a large sphere [31], of the gas-to-soliton crossover [32], and of the anyonic spectrum on the sphere [33,34]. These developments address the fundamental theoretical issue of understanding few-body physics in curved geometries and are potentially interesting for experiments with shell-shaped gases [35–38] and with other low-dimensional curved geometries [39].

In this Letter, we calculate the energy and wave function of two atoms confined to a sphere varying the scattering length a and the total angular momentum j. Technically, at fixed j the problem is reduced to a finite set of coupled differential equations for the relative wave function. We derive these equations by adapting to our case the rigid-rotor formalism of Ref. [29]. We find that, for a small dimer, when a is much smaller than $R/\sqrt{j}$ (R is the sphere radius), the wave function is well approximated by the product of the isotropic relative wave function, the same as in the flat case, and the wave function of the center-of-mass motion with angular momentum j. However, upon increasing a (or j) the dimer becomes anisotropic; the relative wave function gets more and more squeezed in the direction perpendicular to the direction of the center-of-mass motion. We argue that this squeezing is due to an effective harmonic confinement with oscillator length $\sim R/\sqrt{j}$ acting on the relative degree of freedom. For large j our two-body problem on a sphere can be reduced to a flat-space quasi-one-dimensional problem in this effective harmonic confinement. The two-body state can be of localized or delocalized character and it can be two dimensional or quasi one dimensional depending on the relationships among the three relevant length scales a, R, and $R/\sqrt{j}$. In the rest of the Letter we use the sphere radius as the unit of length, i.e., we set $R = 1$.

Our two-body system on a sphere has four angular degrees of freedom, which admit different parametrizations. We first work with the center-of-mass and relative angles $\vec{u} = (\alpha, \beta, \gamma, \theta)$. Figure 1 shows how the set $\vec{u}$ is related to the single-particle vectors $\vec{r}_1$ and $\vec{r}_2$ (see the Supplemental Material for explicit expressions [40]). The spherical coordinates $\alpha \in [0, 2\pi]$ and $\beta \in [0, \pi]$ parametrize the center-of-mass vector $\vec{n}_c = (\vec{r}_1 + \vec{r}_2)/|\vec{r}_1 + \vec{r}_2|$. The relative vector $\vec{n}_r = (\vec{r}_1 - \vec{r}_2)/|\vec{r}_1 - \vec{r}_2|$ is parametrized by α, β, and by the an-

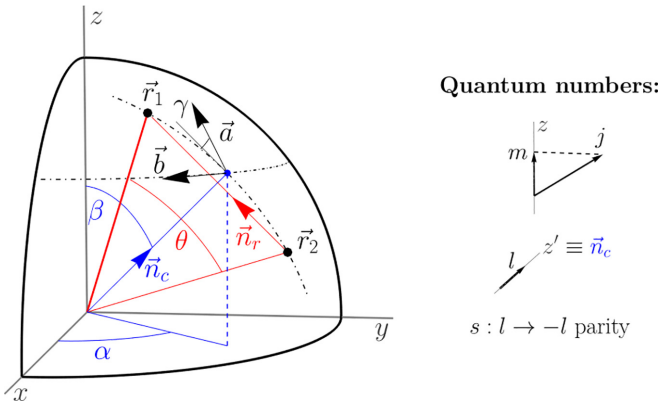

FIG. 1. Illustration of the coordinate system of two particles located at $\vec{r}_1$ and $\vec{r}_2$. Their geodesic center of mass, pointed by the vector $\vec{n}_c$ is described by the spherical coordinates α and β, while their relative position, pointed by the vector $\vec{n}_r$, is described by the angles γ and θ. The system is characterized by four quantum numbers: the total angular momentum j, its projection m along the axis z, the angular momentum l describing the molecular rotation along the $z' = \vec{n}_c$ axis, and the parity s of the eigenstates under the exchange $l \to -l$.

gle $\gamma \in [0, 2\pi]$ between the geodesic passing by the center of mass and the great circle passing by the north pole. Finally, $\theta \in [0, \pi]$ is the relative angular distance between the atoms.

The Schrödinger equation for the two-body wave function $\Psi(\alpha, \beta, \gamma, \theta)$ reads

$$(\hat{T} - E)\Psi = 0, \tag{1}$$

where the relation between the two-body energy E and the s-wave scattering length a is obtained by imposing the Bethe-Peierls boundary condition $\Psi|_{\theta\to 0} \propto \ln(\theta/a)$. The kinetic-energy operator $\hat{T}$ is derived by directly calculating the Laplace-Beltrami operator in the coordinates $\vec{u}$, finding (see the Supplemental Material for details [40]) $\hat{T} = (\hat{J}^2_{x'}/I_{x'} + \hat{J}^2_{y'}/I_{y'} + \hat{J}^2_{z'}/I_{z'})/2 + \hat{L}^2_\theta$, which is the sum of the rotational energies along the molecular axes $(\vec{x}\,', \vec{y}\,', \vec{z}\,') = (\vec{n}_r, \vec{n}_c \times \vec{n}_r, \vec{n}_c)$ and of the kinetic energy $\hat{L}^2_\theta = -(\sin\theta)^{-1}\partial_\theta(\sin\theta\,\partial_\theta)$ for the relative motion along θ [30]. The moments of inertia are equal to $I_{x'} = 2\cos^2(\theta/2)$, $I_{y'} = 2$, and $I_{z'} = 2\sin^2(\theta/2)$, while the expressions of the angular-momentum operators $\hat{J}_{x'}$, $\hat{J}_{y'}$, and $\hat{J}_{z'}$ in terms of α, β, and γ are reported in the Supplemental Material [40]. We now rewrite $\hat{T}$ through the total angular-momentum operator $\hat{J}^2 = \hat{J}^2_{x'} + \hat{J}^2_{y'} + \hat{J}^2_{z'}$ and the ladder operators $\hat{J}_\pm = \hat{J}_{x'} \pm i\hat{J}_{y'}$, obtaining

$$\hat{T} = A(\theta)\hat{J}^2 + B(\theta)\hat{J}^2_{z'} + C(\theta)(\hat{J}^2_+ + \hat{J}^2_-) + \hat{L}^2_\theta, \tag{2}$$

with $A(\theta) = [1/\cos^2(\theta/2) + 1]/8$, $B(\theta) = [8/\sin^2\theta - 1 - 3/\cos^2(\theta/2)]/8$, and $C(\theta) = \tan^2(\theta/2)/16$. The common eigenstates of $\hat{J}^2$ and $\hat{J}_{z'}$ are the Wigner-D matrices $D^{j*}_{ml}(\alpha, \beta, \gamma)$ [41], satisfying the relations

$$\begin{aligned} \hat{J}^2 D^{j*}_{ml} &= j(j+1)D^{j*}_{ml}, \\ \hat{J}^2_{z'} D^{j*}_{ml} &= l^2 D^{j*}_{ml}, \\ \hat{J}_\pm D^{j*}_{ml} &= [j(j+1) - l(l\pm 1)]^{1/2} D^{j*}_{ml\pm 1}. \end{aligned} \tag{3}$$

These eigenstates are labeled by the total angular momentum j, by its projection along the z axis $m = -j, \ldots, j$, and by the angular-momentum projection along the z' axis $l = -j, \ldots, j$ (see Fig. 1). Note that the operator $\hat{T}$ conserves j and m, but it does couple states with l different by 2. We decompose the wave function in each j, m channel as [5,42]

$$\Psi_{j,m}(\alpha, \beta, \gamma, \theta) = \sum_{\substack{l=0,\\ l\ \text{even}}}^{j} \psi_l(\theta) S_{jml}(\alpha, \beta, \gamma), \tag{4}$$

where $S_{jml} = (D^{j*}_{ml} + D^{j*}_{m-l})/\sqrt{2}$ for $l > 0$, while $S_{jm0} = D^{j*}_{m0}$, and using the properties (3) we reduce Eq. (1) to

$$\begin{aligned} &\left[\hat{L}^2_\theta + j(j+1)A(\theta) + l^2 B(\theta)\right]\psi_l(\theta) \\ &\quad + C(\theta)[c_l\psi_{l+2}(\theta) + c_{l-2}\psi_{l-2}(\theta)] = E_j\psi_l(\theta), \end{aligned} \tag{5}$$

where $c_l = \sqrt{(j-l-1)(j-l)(j+l+1)(j+l+2)}$, $c_0 = \sqrt{2(j-1)j(j+1)(j+2)}$, and $c_l = 0$ for $l < 0$. Note that we only include the even-l wave function components in Eq. (4) because the operator $\hat{T}$ does not couple even-l channels to odd-l channels. Indeed, for zero-range s-wave interaction the odd-l part describes noninteracting states and we are only interested in the even-l channels (the p-wave-interacting case has been considered in Ref. [29]). In fact, the s-wave interaction is effective only in the equation with $l = 0$ because the other components experience the centrifugal barrier $l^2B(\theta) \propto 1/\theta^2$. Also note that $\hat{T}$ conserves parity under the exchange $l \to -l$. While the odd-parity configurations are insensitive to the interaction, the symmetric states under this exchange feel the interaction through their coupling to ψ_0. By expanding the wave function in terms of symmetric superpositions of opposite l channels, S_{jlm}, we select only the even-parity configurations. Thus, our dimer problem with s-wave interaction essentially reduces to $(j+2)/2$ coupled differential equations for even j or to $(j+1)/2$ equations for odd j (recall that $|l| \leqslant j$).

In particular, for $j = 0$ we have the single equation $(\hat{L}^2_\theta - E_0)\psi_0(\theta) = 0$, solved in terms of Legendre functions [32,43]: $\psi_0(\theta) \propto P_{-1/2+s}[\cos(\pi - \theta)]$, with $s = (E_0 + 1/4)^{1/2}$. The energy E_0 is then obtained from $\ln(1/a) = [\mathcal{D}(1/2+s) + \mathcal{D}(1/2-s)]/2 + \ln(e^{\gamma_E}/2)$, where $\mathcal{D}$ is the digamma function and γ_E is the Euler-Mascheroni constant.

The case $j = 1$ is governed by a different but also single equation $[\hat{L}^2_\theta + 2A(\theta) - E_1]\psi_0(\theta) = 0$, which can be rewritten in the form of the Jacobi differential equation. We obtain its solution in terms of Jacobi functions $\psi_0(\theta) \propto (1 + \cos\theta)^{-1/2} J^{(-1,0)}_\nu[\cos(\pi - \theta)]$, with $\nu = E_1^{1/2}$ [44]. The Bethe-Peierls boundary condition leads to the relation between the energy and the scattering length: $\ln(1/a) = [\mathcal{D}(\nu) + \mathcal{D}(-\nu)]/2 + \ln(e^{\gamma_E}/2)$.

For $j > 1$ we solve Eq. (5) numerically. The energies E_j as functions of a are presented in Fig. 2 as solid curves. The dashed curves correspond to the two leading-order terms in the expansion of the energy in powers of small a:

$$E_j^{(a\ll 1)} = E^{(\text{flat})} - 1/3 + j(j+1)/4, \tag{6}$$

where $E^{(\text{flat})} = -4\exp(-2\gamma_E)/a^2$ is the dimer energy in the flat case. The center-of-mass energy $j(j+1)/4$ and the leading-order curvature-induced shift $-1/3$ can be obtained

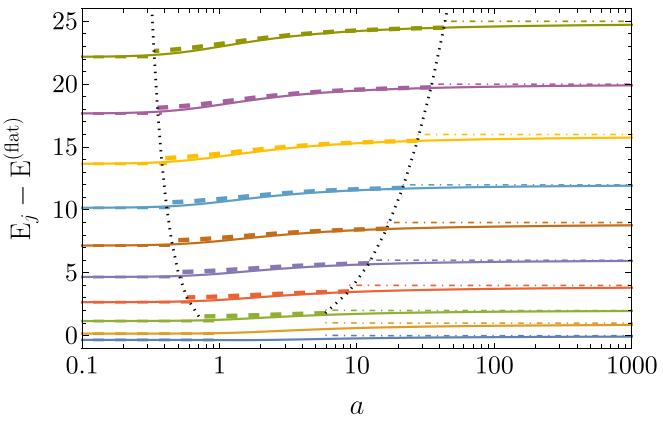

FIG. 2. Dimer energy spectrum versus a for $j = 0, \ldots, 9$ (continuous lines). The exact curves converge towards the analytical asymptotes of Eqs. (6) and (7) valid, respectively, in the strongly attractive regime $a \ll 1$ (dashed lines), and in the noninteracting regime $a \gg 1$ (dot-dashed lines). In the intermediate a regime, the curves are well reproduced by the semi-analytical quasi-one-dimensional theory (thick dashed lines). The dimer is quasi-one-dimensional between the dotted curves; the left border corresponds to the dimer aspect ratio ≈ 1 and the right border indicates where the dimer size becomes comparable to the sphere radius (see text).

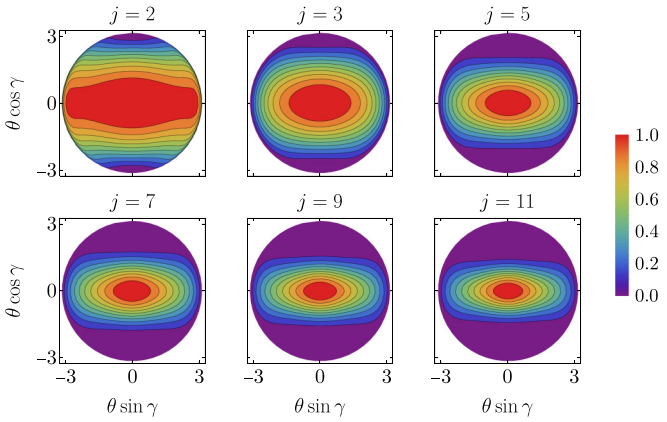

FIG. 3. Contour plots of the ratio (rescaled to its maximum) $|\Psi_{j,m}(\alpha, \pi/2, \gamma, \theta)/K_0(2e^{-\gamma_E}\theta/a)|$ for $a = 2$, which demonstrate the squeezing of the state along the direction of motion of the center of mass.

by solving Eq. (5) perturbatively at small $\theta \sim a$. In doing this it is convenient to rewrite the operator $\hat{L}_\theta^2$ and the functions $A(\theta)$, $B(\theta)$, $C(\theta)$ changing the variable from the angle θ to the chord distance $\rho = 2\sin(\theta/2)$ (see Ref. [32]). The dash-dotted horizontal lines correspond to the formulas

$$\begin{aligned} E_{j\,\mathrm{even}}^{(a\gg 1)} &= j^2/4 + j/2, \\ E_{j\,\mathrm{odd}}^{(a\gg 1)} &= j^2/4 + j/2 + 1/4. \end{aligned} \tag{7}$$

Equations (7) follow from the fact that the energy on the sphere scales quadratically with the angular momentum and, therefore, for fixed total angular momentum j the lowest-energy state of two noninteracting atoms is obtained when their (integer) angular momenta j_1 and j_2 are as close as possible to $j/2$ and are also such that $j_1 + j_2 = j$. In Fig. 2 we show the lowest-energy two-body states for fixed total angular momenta j. These energies do not depend on the projection, which can be $m = -j, \ldots, j$. Note that we assume the thin-shell regime completely neglecting the degree of freedom perpendicular to the sphere surface (see Ref. [45] for an analysis of the case where the radial excitations are not frozen and where angular and radial degrees of freedom are coupled).

We now discuss how the wave function depends on j. For $j = 0$ and $j = 1$ only ψ_0 is nonzero and the total wave function is independent of γ, which can be seen from Eq. (4) bearing in mind that $S_{000} = 1$ and $S_{110} = e^{-i\alpha}\sin\beta/\sqrt{2}$. The dimer in these cases is isotropic although the θ dependence of its wave function is sensitive to j. The anisotropy first appears in the case $j = 2$ where $\psi_2 \neq 0$. It manifests itself in a squeezing of the molecule along a direction which depends on the center-of-mass angles α and β and on m (note, however, that ψ_l depend on j, but not on m). The phenomenon can be seen clearly in the case $m = j$, which corresponds to the center-of-mass motion of the molecule along the equator. If we also set the center of mass on the equator ($\beta = \pi/2$), the wave function (4) explicitly reads $\Psi_{j,j}(\alpha, \pi/2, \gamma, \theta) \propto e^{-ij\alpha}[\psi_0(\theta)/j! + \sum_{l>0}\psi_l(\theta)\cos(l\gamma)/\sqrt{2(j+l)!(j-l)!}]$. We demonstrate the squeezing of the dimer by plotting the quantity $|\Psi_{j,j}(\alpha, \pi/2, \gamma, \theta)/\Psi^{(\mathrm{flat})}(\theta)|$ in Fig. 3 for $a = 2$ (note that $|\Psi_{j,j}(\alpha, \pi/2, \gamma, \theta)|$ is independent of α). We divide by the (isotropic) bound-state wave function in the flat-case limit $\Psi^{(\mathrm{flat})}(\theta) = K_0(2e^{-\gamma_E}\theta/a)$ to remove the logarithmic divergence at $\theta \to 0$ and to better visualize the angular distribution of the state. We observe that by increasing j the dimer becomes more and more squeezed in the direction perpendicular to the equator, i.e., perpendicular to the center-of-mass motion.

The squeezing becomes more pronounced for large j. In this case the dimer wave function (4) involves many l components and for describing the system it is more convenient to switch from $(\alpha, \beta, \gamma, \theta)$ to the single-particle bases of polar and azimuthal angles $(\theta_1, \phi_1, \theta_2, \phi_2)$. As we have already mentioned, for fixed j (let us assume for simplicity that j is even), two noninteracting atoms prefer to occupy single-particle orbitals with angular momenta $j_1 = j_2 = j/2$. If $m = j$, we also have $m_1 = m_2 = j/2$. For large j such orbitals are localized close to the equator of the sphere where $\theta_\sigma \approx \pi/2$. The variation of θ_σ is of order $|\theta_\sigma - \pi/2| \sim 1/\sqrt{j}$. One can see this by switching to the variable $y_\sigma = \theta_\sigma - \pi/2$ and observing that the single-particle kinetic-energy operator can be written as $[-\partial^2/\partial y_\sigma^2 + \tan y_\sigma \partial/\partial y_\sigma + j^2/(4\cos^2 y_\sigma)]/2$. The expansion of $j^2/8\cos^2 y_\sigma$ at small y_σ gives an approximately harmonic potential with frequency $j/2$ which localizes the wave function to the oscillator length $\sqrt{2/j}$. As we show in the Supplemental Material [40], this localization persists also in the interacting case. The dimer problem becomes quasi-one-dimensional and the dimer energy $E = j^2/4 + j/2 + q^2$ is obtained by solving

$$\int_0^\infty e^{2q^2\tau/j}\left(\sqrt{\tau/\sinh\tau}\,e^{\tau/2} - 1\right)\frac{d\tau}{4\pi\tau} = \frac{1}{2\pi}\ln\frac{\sqrt{-q^2}ae^{\gamma_E}}{2}. \tag{8}$$

The corresponding results are shown as dashed curves in Fig. 2. Equation (8) is valid for $j = m \gg 1$ and we require $1 \ll -q^2 \lesssim j$ (see more details in the Supplemental Material [40]). Under these conditions the two-body wave function is well approximated by $\Psi(\theta_1, \phi_1, \theta_2, \phi_2) \approx \exp[-j(\theta_1 - \pi/2)^2/4 - j(\theta_2 - \pi/2)^2/4 - (-q^2)^{1/2}|\phi_1 - \phi_2|]$, its quasi-one-dimensional character is explicit; in the direction of the center-of-mass motion the dimer has the size $1/(-q^2)^{1/2}$ which is larger than its width given by $\approx 1/\sqrt{j}$.

We can now summarize the main regimes of an s-wave-interacting dimer on a sphere. For small j, with increasing a the dimer increases in size but remains to a large extent isotropic. The change of the character in this case happens at $a \approx 1$ when the dimer size becomes comparable to the sphere radius. For large j we identify the following three regimes: For $a \lesssim 1/\sqrt{j}$ the dimer is strongly bound and approximately isotropic. In the interval $1/\sqrt{j} \lesssim a \lesssim a^*$ the dimer is quasi-one-dimensional and its size is smaller than the sphere radius. The characteristic scattering length $a^* \approx e^{\sqrt{\pi j/2}}$ is obtained by setting $q^2 = -1$ in Eq. (8). It marks the crossover to the third regime where the two atoms are delocalized along the equator but localized in the perpendicular direction with polar angles $|\theta_\sigma - \pi/2| \sim 1/\sqrt{j}$. The dotted curves in Fig. 2 correspond to $a = 1/\sqrt{j}$ (left border) and $a = a^*$ (right border) and indicate the regime where the dimer is quasi-one-dimensional.

In conclusion, we find the spectrum and wave functions of an s-wave-interacting dimer on a spherical surface as a function of the scattering length a and total angular momentum j. The nonseparability of the relative and center-of-mass degrees of freedom manifests itself in squeezing of the dimer in the direction transversal to the center-of-mass motion. The effect is most pronounced for $a \gtrsim 1/\sqrt{j}$ when the dimer becomes quasi-one-dimensional. Moreover, for $a \gg 1$, when the attraction is insufficient to localize two atoms into a dimer at low j, this transversal squeezing enhances the attraction and eventually leads to a bound quasi-one-dimensional dimer at sufficiently large j.

Our findings have implications for ongoing experiments with shell-shaped magnetic [35,36,46] and optical [37,38] traps as well as for proposals based on quantum effects in self-bound mixtures [47]. One can be able to create rapidly rotating gases by combining gravity-compensation mechanisms with phase-imprinting techniques for transferring angular momentum to the gas [48,49]. The two-body spectrum that we calculate can be measured experimentally by radio-frequency spectroscopy [11,12] and the anisotropy of the dimers can be observed in time-of-flight experiments. If we neglect interactions, after a long free expansion, the distribution of atoms is directly related to the Fourier transform of the original wave function. The free expansion of shell-shaped gases in their ground states at zero angular momentum has been analyzed in Refs. [36,37,50,51]. In the future, to account for trap imperfections (gravitational sag, ellipticity, local variations of the curvature, finite shell thickness and its variations, etc.) we think of generalizing our harmonic large-j theory to a finite out-of-surface confinement and to generic nonspherical geometries. From the many-body perspective, we can mention the study of the BCS-BEC crossover on a sphere [52], which would be interesting to reconsider at a finite angular momentum, and the gas-to-soliton transition for attractive bosons [32]. This transition is characterized by a subtle interplay among the space curvature, mean-field and beyond-mean-field effects, and we believe that it should also be sensitive to the total angular momentum.

A.T. acknowledges financial support of the Horizon Europe programme HORIZON-CL4-2022-QUANTUM-02-SGA via the Project No. 101113690 (PASQuanS2.1). The ICFO-QOT group acknowledges support from the European Research Council AdG NOQIA; MCIN/AEI [PGC2018-0910.13039/501100011033, CEX2019-000910-S/10.13039/501100011033, Plan National FIDEUA PID2019-106901GB-I00, Plan National STAMEENA PID2022-139099NB-I00, project funded by MCIN/AEI/10.13039/501100011033 and by the "European Union NextGenerationEU/PRTR" (PRTR-C17.I1), FPI]; QUANTERA DYNAMITE PCI2022-132919, QuantERA II Programme co-funded by European Union's Horizon 2020 program under Grant Agreement No. 101017733; Ministry for Digital Transformation and of Civil Service of the Spanish Government through the QUANTUM ENIA project call - Quantum Spain project, and by the European Union through the Recovery, Transformation and Resilience Plan - NextGenerationEU within the framework of the Digital Spain 2026 Agenda; Fundació Cellex; Fundació Mir-Puig; Generalitat de Catalunya (European Social Fund FEDER and CERCA program; Barcelona Supercomputing Center MareNostrum (FI-2023-3-0024); Funded by the European Union. Views and opinions expressed are however those of the author(s) only and do not necessarily reflect those of the European Union, European Commission, European Climate, Infrastructure and Environment Executive Agency (CINEA), or any other granting authority. Neither the European Union nor any granting authority can be held responsible for them (HORIZON-CL4-2022-QUANTUM-02-SGA PASQuanS2.1, 101113690, EU Horizon 2020 FET-OPEN OPTOlogic, Grant No 899794, QU-ATTO, 101168628). EU Horizon Europe Program (This project has received funding from the European Union's Horizon Europe research and innovation program under Grant Agreement No. 101080086 NeQSTGrant Agreement 101080086—NeQST); ICFO Internal "QuantumGaudi" project.

Data availability. The data that support the findings of this article are openly available [54].

[1] A. Einstein, L. Infeld, and B. Hoffmann, The gravitational equations and the problem of motion, Ann. Math. **39**, 65 (1938).

[2] B. M. Barker and R. F. O'Connell, Gravitational two-body problem with arbitrary masses, spins, and quadrupole moments, Phys. Rev. D **12**, 329 (1975).

[3] A. Buonanno and T. Damour, Effective one-body approach to general relativistic two-body dynamics, Phys. Rev. D **59**, 084006 (1999).

[4] A. Schild, Electromagnetic two-body problem, Phys. Rev. **131**, 2762 (1963).

[5] L. D. Landau and E. M. Lifshitz, *Quantum Mechanics* (Butterworth-Heinemann, Oxford 1981).

[6] F. Dalfovo, S. Giorgini, L. P. Pitaevskii, and S. Stringari, Theory of Bose-Einstein condensation in trapped gases, Rev. Mod. Phys. **71**, 463 (1999).

[7] S. Giorgini, L. P. Pitaevskii, and S. Stringari, Theory of ultracold atomic Fermi gases, Rev. Mod. Phys. **80**, 1215 (2008).

[8] M. Olshanii, Atomic scattering in the presence of an external confinement and a gas of impenetrable bosons, Phys. Rev. Lett. **81**, 938 (1998).

[9] D. S. Petrov and G. V. Shlyapnikov, Interatomic collisions in a tightly confined Bose gas, Phys. Rev. A **64**, 012706 (2001).

[10] T. Busch, B. G. Englert, K. Rzażewski, and M. Wilkens, Two cold atoms in a harmonic trap, Found. Phys. **28**, 549 (1998).

[11] T. Stöferle, H. Moritz, K. Günter, M. Köhl, and T. Esslinger, Molecules of fermionic atoms in an optical lattice, Phys. Rev. Lett. **96**, 030401 (2006).

[12] G. Thalhammer, K. Winkler, F. Lang, S. Schmid, R. Grimm, and J. Hecker Denschlag, Long-lived Feshbach molecules in a three-dimensional optical lattice, Phys. Rev. Lett. **96**, 050402 (2006).

[13] Edited by W. Zwerger, *The BCS-BEC Crossover and the Unitary Fermi Gas* (Springer, Berlin, Heidelberg, 2011), Vol. 836.

[14] C.-L. Hung, X. Zhang, N. Gemelke, and C. Chin, Observation of scale invariance and universality in two-dimensional Bose gases, Nature (London) **470**, 236 (2011).

[15] T. Yefsah, R. Desbuquois, L. Chomaz, K. J. Günter, and J. Dalibard, Exploring the thermodynamics of a two-dimensional Bose gas, Phys. Rev. Lett. **107**, 130401 (2011).

[16] B. Bakkali-Hassani, C. Maury, Y.-Q. Zou, E. Le Cerf, R. Saint-Jalm, P. C. M. Castilho, S. Nascimbene, J. Dalibard, and J. Beugnon, Realization of a Townes soliton in a two-component planar Bose gas, Phys. Rev. Lett. **127**, 023603 (2021).

[17] C.-A. Chen and C.-L. Hung, Observation of scale invariance in two-dimensional matter-wave Townes solitons, Phys. Rev. Lett. **127**, 023604 (2021).

[18] P. O. Fedichev, M. J. Bijlsma, and P. Zoller, Extended molecules and geometric scattering resonances in optical lattices, Phys. Rev. Lett. **92**, 080401 (2004).

[19] P.-I. Schneider, S. Grishkevich, and A. Saenz, *Ab initio* determination of Bose-Hubbard parameters for two ultracold atoms in an optical lattice using a three-well potential, Phys. Rev. A **80**, 013404 (2009).

[20] P. Massignan and Y. Castin, Three-dimensional strong localization of matter waves by scattering from atoms in a lattice with a confinement-induced resonance, Phys. Rev. A **74**, 013616 (2006).

[21] Y. Nishida and S. Tan, Universal Fermi gases in mixed dimensions, Phys. Rev. Lett. **101**, 170401 (2008).

[22] G. Lamporesi, J. Catani, G. Barontini, Y. Nishida, M. Inguscio, and F. Minardi, Scattering in mixed dimensions with ultracold gases, Phys. Rev. Lett. **104**, 153202 (2010).

[23] D. Xiao, R. Zhang, and P. Zhang, Confinement induced resonance with weak bare interaction in a quasi $3+0$ dimensional ultracold gas, Few-Body Syst. **60**, 63 (2019).

[24] E. L. Bolda, E. Tiesinga, and P. S. Julienne, Ultracold dimer association induced by a far-off-resonance optical lattice, Phys. Rev. A **71**, 033404 (2005).

[25] S. Sala and A. Saenz, Theory of inelastic confinement-induced resonances due to the coupling of center-of-mass and relative motion, Phys. Rev. A **94**, 022713 (2016).

[26] V. Peano, M. Thorwart, C. Mora, and R. Egger, Confinement-induced resonances for a two-component ultracold atom gas in arbitrary quasi-one-dimensional traps, New J. Phys. **7**, 192 (2005).

[27] V. Melezhik and P. Schmelcher, Quantum dynamics of resonant molecule formation in waveguides, New J. Phys. **11**, 073031 (2009).

[28] A. Tononi and L. Salasnich, Low-dimensional quantum gases in curved geometries, Nat. Rev. Phys. **5**, 398 (2023).

[29] Z.-Y. Shi and H. Zhai, Emergent gauge field for a chiral bound state on curved surface, J. Phys. B: At. Mol. Opt. Phys. **50**, 184006 (2017).

[30] J. Zhang and T.-L. Ho, Potential scattering on a spherical surface, J. Phys. B: At. Mol. Opt. Phys. **51**, 115301 (2018).

[31] A. Tononi, Scattering theory and equation of state of a spherical two-dimensional Bose gas, Phys. Rev. A **105**, 023324 (2022).

[32] A. Tononi, G. E. Astrakharchik, and D. S. Petrov, Gas-to-soliton transition of attractive bosons on a spherical surface, AVS Quantum Sci. **6**, 023201 (2024).

[33] S. Ouvry and A. P. Polychronakos, Anyons on the sphere: Analytic states and spectrum, Nucl. Phys. B **949**, 114797 (2019).

[34] A. P. Polychronakos and S. Ouvry, Two anyons on the sphere: Nonlinear states and spectrum, Nucl. Phys. B **951**, 114906 (2020).

[35] Y. Guo, R. Dubessy, M. de Goër de Herve, A. Kumar, T. Badr, A. Perrin, L. Longchambon, and H. Perrin, Supersonic rotation of a superfluid: A long-lived dynamical ring, Phys. Rev. Lett. **124**, 025301 (2020).

[36] R. A. Carollo, D. C. Aveline, B. Rhyno, S. Vishveshwara, C. Lannert, J. D. Murphree, E. R. Elliott, J. R. Williams, R. J. Thompson, and N. Lundblad, Observation of ultracold atomic bubbles in orbital microgravity, Nature (London) **606**, 281 (2022).

[37] F. Jia, Z. Huang, L. Qiu, R. Zhou, Y. Yan, and D. Wang, Expansion dynamics of a shell-shaped Bose-Einstein condensate, Phys. Rev. Lett. **129**, 243402 (2022).

[38] Z. Huang, K. Y. Lee, C. K. Wong, L. Qiu, B. Yang, Y. Yan, and D. Wang, Probing the hollowing transition of a shell-shaped BEC with collective excitation, arXiv:2503.12318.

[39] T. Fernholz, R. Gerritsma, P. Krüger, and R. J. C. Spreeuw, Dynamically controlled toroidal and ring-shaped magnetic traps, Phys. Rev. A **75**, 063406 (2007).

[40] See Supplemental Material at http://link.aps.org/supplemental/10.1103/PhysRevA.111.L051304 for additional details on the coordinate system, on the kinetic energy operator, and on the derivation of Eq. (8) of the Letter, which also includes Ref. [53].

[41] D. A. Varshalovich, A. N. Moskalev, and V. K. Khersonskii, *Quantum Theory of Angular Momentum* (World Scientific, Singapore, 1988).

[42] W. Gordy and R. L. Cook, *Microwave Molecular Spectra*, 3rd ed. (Wiley, New York, 1984), Chap. VII.2.

[43] I. Fedotova and N. Virchenko, *Generalized Associated Legendre Functions and Their Applications* (World Scientific Publishing, Singapore, 2001).

[44] We thank one of the referees for suggesting this form. Originally we reported the $j = 1$ solution in terms of hypergeometric functions.

[45] C. M. Carmesin and M. A. Efremov, Confinement induced resonances in spherical shell traps, arXiv:2401.14946.

[46] A. Beregi, C. Foot, and S. Sunami, Quantum simulations with bilayer 2D Bose gases in multiple-RF-dressed potentials featured, AVS Quantum Sci. **6**, 030501 (2024).

[47] Y. Ma and X. Cui, Shell-shaped quantum droplet in a three-component ultracold Bose gas, Phys. Rev. Lett. **134**, 043402 (2025).

[48] R. Sharma, D. Rey, L. Longchambon, A. Perrin, H. Perrin, and R. Dubessy, Thermal melting of a vortex lattice in a quasi-two-dimensional Bose gas, Phys. Rev. Lett. **133**, 143401 (2024).

[49] R. Dubessy and H. Perrin, Perspective: Quantum gases in bubble traps, AVS Quantum Sci. **7**, 010501 (2025).

[50] C. Lannert, T.-C. Wei, and S. Vishveshwara, Dynamics of condensate shells: Collective modes and expansion, Phys. Rev. A **75**, 013611 (2007).

[51] A. Tononi, F. Cinti, and L. Salasnich, Quantum bubbles in microgravity, Phys. Rev. Lett. **125**, 010402 (2020).

[52] Y. He, H. Guo, and C.-C. Chien, BCS-BEC crossover of atomic Fermi superfluid in a spherical bubble trap, Phys. Rev. A **105**, 033324 (2022).

[53] R. P. Feynman and A. R. Hibbs, *Quantum Mechanics and Path Integrals* (McGraw-Hill, New York, 1965).

[54] A. Tononi, Data from Fig. 2 of arXiv:2502.06724, Zenodo (2025), https://zenodo.org/records/15275846.